Dynamics of the radiative recombination in cylindrical nanostructures with type-II band alignment

V. A. Shuvayev,[1] I. L. Kuskovsky,[1] L. I. Deych,[1] Y. Gu,[2] Y. Gong,[3] G. F. Neumark,[3] M. C. Tamargo,[4] and A. A. Lisyansky[1]
[1]*Department of Physics, Queens College of the City University of New York, Flushing, New York 11367, USA*
[2]*Department of Physics and Astronomy, Materials Science Program, Washington State University, Pullman, Washington 99164, USA*
[3]*Department of Applied Physics and Applied Mathematics, Columbia University, New York, New York 10027, USA*
[4]*Department of Chemistry, City College of the City University of New York, New York, New York 10036, USA*
(Received 6 June 2008; revised manuscript received 4 February 2009; published 11 March 2009)

The electron and hole states and confining potential for cylindrical core-shell structure with type-II band alignment are obtained from a numerical solution of the self-consistent Schrödinger-Poisson system of equations. The photoluminescence (PL) kinetics is theoretically analyzed, with the nanostructure size dispersion taken into account. The results are applied to the radiative recombination in the system of ZnTe/ZnSe stacked quantum dots. A good agreement with both cw and time-resolved experimental observations is found. It is shown that size distribution results in the PL decay that has essentially nonexponential behavior even at the tail of the decay where the carrier lifetime is almost the same due to slowly changing overlap of the electron and hole wave functions. Finally, a model situation applicable to colloidal core-shell nanowires is investigated and discussed.

DOI: 10.1103/PhysRevB.79.115307 PACS number(s): 78.67.Lt, 73.21.Hb, 78.47.Cd

I. INTRODUCTION

One-dimensional (1D) nanoscale structures such as quantum wires (QWRs) have been attracting a great deal of interest due to their potential for applications in various electronic and optical devices, such as transistors, diodes, lasers, and biological sensors (see, e.g., Refs. 1–3 and references therein). This interest is further stimulated by recent advances in fabrication technologies that led to development of several growth techniques allowing synthesizing QWR composed of two single-crystalline semiconductor materials with core shell, core multishell, or superlatticelike structure.[4,5] Heterojunctions formed in these structures result in the band discontinuities whose effect on spectrum of electrons and holes in the effective-mass approximation can be described in terms of effective potential wells and barriers for carriers residing in different materials. If the band alignment produces potential wells for both electrons and holes within the same material, the structure is classified as type-I. Another type of band alignment, called type-II, results in formation of the potential well for electrons in one material and for holes in the other. As a result, electrons and holes in type-II structures are spatially separated giving rise to an internal electric field that bends the conduction and valence bands and modifies energy levels and wave functions of electron-hole pairs. This effect is manifested in both cw and time-resolved photoluminescence (PL): in the former it is responsible for the blueshift of the PL with increasing excitation intensity,[6–11] whereas in the latter it results in a relatively long (due to weak overlap of the wave functions) nonexponential decay,[6,9,10] which also depends on the excitation intensity.[6,9–11] There have been a number of attempts to obtain a quantitative description of this behavior in type-II quantum wells using self-consistent Poisson-Schrödinger analysis[6] or microscopical multiband semiconductor luminescence equations.[11]

In this paper we focus on theoretical studies of similar effects in type-II cylindrical heterostructures characterized by two-dimensional confinement of the carriers. In our calculations, based on self-consistent Schrödinger-Poisson equations, we study dependence of electron and hole energies and wave functions on the number of photoexcited carriers taking into account a possibility of population of not only the ground but also excited electron and hole states. The results of these calculations are used to model dependence of cw PL energies on the excitation intensity as well as behavior of time-resolved PL. In the latter case, we take into account that the experimentally observed nonexponential tail in the time dependence of the PL may be caused not only by modifications of the electron-hole states dependent on excitation intensity, but also by random variations in geometric characteristics (e.g., size) of nanostructures. Such a dependence on geometry arises because in a typical PL experiment the signal is collected from a large number of nanostructures. This effect is often considered by fitting experimental results to multiexponential[12] or stretch-exponential[13] function with fitting parameters having little if any physical meaning. Here we take into account effects of the disorder by directly averaging the calculated intensity of emission over a statistical distribution of the parameters of the considered structures, following the approach of Ref. 14. Taking into account both effects contributing to the nonexponential PL decay enables us to carry out more accurate comparison of our calculations with experimental results.

While our calculations most directly apply to quantum wires with a small modification they can also be used to study different types of structures with cylindrical symmetry. In particular, we use our approach to explain results of cw and time-resolved PL measurements performed on vertically stacked self-assembled quantum dots (QDs) with close to a circular cross section. Although this system differs from quantum wires, we show that under certain circumstances one can easily adapt our theory by introducing an anisotropic effective mass for holes. In Sec. II we discuss our model, describe details of calculations, and provide more detailed

arguments justifying applicability of our results to vertically stacked quantum dot structures. Details of the experimentally studied structure and comparison of the theory and experimental results are described in Sec. III, which is followed by a summary.

II. THEORETICAL MODEL AND CALCULATIONS

A. Self-consistent potential, energy levels, and wave functions

The theoretical analysis is based on an assumption that high-energy electron-hole pairs created by an optical pulse rapidly relax into the lowest available states by nonradiative processes, where they reach a quasiequilibrium with the lattice before they recombine radiatively. Therefore, populations of electrons and holes can be characterized by the Fermi distributions with two independent chemical quasipotentials. The goal of theoretical calculations in this situation is to find the electron and hole Fermi levels as functions of the number of excited electron-hole pairs. To this end we solve the Schrödinger equations for electrons and holes with the Coulomb interaction taken into account within a Hartree approximation. Within this approximation the confinement potential is combined with an electrostatic potential $\phi(r)$ determined self-consistently from the Poisson equation. In our model the nanostructure is taken as an infinitely long cylindrical type-II core-shell quantum wire with shell radius r_s and core radius r_c.

The applicability of this model to vertically stacked QDs, studied experimentally (Sec. III), requires additional justifications, which are different for electrons and holes. Electrons in this structure reside outside the dots in the barrier material (ZnSe) and away from the spatial regions above or below the QDs.[15] Therefore, they are virtually free to move in the vertical direction, along the whole stack, and are characterized by an effective mass typical for the bulk ZnSe. This behavior of electrons is confirmed by the experimental observation of the Aharonov-Bohm oscillations in magneto-optical experiments.[15,16] The situation with holes is more complicated. First of all, in these materials the hole ground states are degenerate, so that one has to distinguish between heavy holes and light holes. It is well known that in quantum wires ground state is populated mostly by light holes while in disklike QDs the heavy hole's population is more prevalent.[17,18] The main difference between heavy and light holes (apart from their masses) is that they obey different selection rules for interaction with light. However, this difference manifests itself mostly in polarization-sensitive and magneto-optical experiments. In the phenomena discussed in this paper polarization effects do not play a role, so that we can treat light and heavy holes in a similar way taking into account only difference in their masses and confinement potentials. Another important property of holes in stacked QDs is that, unlike electrons, they are well confined within individual QDs (ZnTe) with only exponential tails of their wave functions "leaking" outside. Using a tight-binding-like arguments one can describe holes in this situation as belonging to a narrow band of propagating states with an effective mass, which is significantly larger than the bulk effective mass. In principle, the value of the "vertical" effective mass can be found using overlap integrals between adjacent QDs, but our calculations showed that its exact value is not important for the system considered in this work. One can think of this situation as of bands of particles with infinite effective mass, so that the respective densities of states become proportional to respective δ functions with a prefactor determined by the number of QDs in the system. Since the luminescence is excited uniformly in the entire stack, we can assume that the holes are also uniformly distributed between QDs. This assumption is consistent with experimentally observed linear dependence of the PL intensity on excitation intensity.[15] In our calculations, however, we use the standard one-dimensional density of states for both holes and electrons and verify that an error due to lack of accurate knowledge of this parameter is smaller than errors caused by uncertainty of the band offsets determining confinement potentials.

We further neglect in our calculations exciton corrections to energies of electron-hole pairs, which is justified due to very small exciton binding energy for these structures (between 2 and 8 meV).[10] Taking into account the mass-mismatch effect, but neglecting valence-band mixing and nonparabolicity of the conduction band, the one-particle Hamiltonian in cylindrical coordinates with polar axis z in the growth direction is given by

$$\hat{H}_j = -\frac{\hbar^2}{2}\left[\frac{1}{r}\frac{\partial}{\partial r}\left(\frac{r}{m_j^*}\frac{\partial}{\partial r}\right) + \frac{1}{m_j^* r^2}\frac{\partial^2}{\partial \theta^2} + \frac{1}{m_{z,j}^*}\frac{\partial^2}{\partial z^2}\right] + V_j(r) + q_j\phi(r), \quad (1)$$

where r and θ are, respectively, radial and azimuthal coordinates, index $j=e,h$ here and throughout the paper refers to electrons and holes, respectively, and q_j is the charge of the particle with $q_h=e$ and $q_e=-e$ with e equal to the electron's charge value. m_j^* stands for electron and hole radial effective masses, while $m_{z,j}^*$ introduces the vertical effective mass, which for electrons coincide with the radial mass, but for holes $m_{z,h}^* \gg m_h^*$. Spatial confining potentials of the conduction and valence bands, V_j, radial effective masses, and the electrostatic potential ϕ depend on the radial coordinate only. The radial effective mass and confining potentials are finite steplike functions with jumps at r_c. In general, in what follows indices c and s are used to designate *core* and *shell* parameters, respectively.

In many papers dealing with heavily doped structures holes are excluded from consideration[19–21] and are replaced with a fixed spatial distribution of the dopants. Such an approach is only justified when the processes under consideration are determined by only one type of carriers. In the case of not intentionally doped structures, similar to the one considered in this paper, the heavy holes significantly contribute to the nonuniform carrier distribution, affecting the potential profile of the structure. Therefore, in this case one has to self-consistently solve both the electron and hole Schrödinger equations, which are coupled through the Poisson potential ϕ.

We separate variables in the Schrödinger equations corresponding to the Hamiltonian by presenting the wave function in the form

$$\Psi_{j,m_j,n_j}(r,\theta,z) = \frac{\psi_{j,m_j,n_j}(r)}{\sqrt{2\pi L_z}} e^{im_j\theta} e^{ik_j z}, \tag{2}$$

where m_j is the azimuthal quantum number, n_j is a radial quantum number, k_j is a wave vector of free motion along the z direction, and L_z is the normalizing length of the wire. At the exterior interface between the shell and vacuum we set $\psi_{j,m_j,n_j}(r_s)=0$, which corresponds to the requirement that the electrons and holes are confined to the volume of the core-shell structure.

The Poisson equation determining the electrostatic potential ϕ for given electron and hole charge densities in undoped materials is given by

$$\frac{1}{r}\frac{\partial}{\partial r}\left(\epsilon(r) r \frac{\partial}{\partial r}\right)\phi = -\frac{e(n_h(r)-n_e(r))}{\epsilon_0}, \tag{3}$$

where $n_e(r)$ and $n_h(r)$ are the electron and hole volume concentrations, which are assumed to depend only on the radial distance r, and $\epsilon(r)$ and ϵ_0 are permittivities of the heterojunction and free space, correspondingly. With $\epsilon(r)$ depending on radial coordinate the effect of the mismatch of dielectric constants is also taken into account. The carrier concentrations are determined by spatial distributions of the wave functions of respective quantum states as follows:

$$n_j(r) = \frac{1}{2\pi}\sum_{m_j,n_j} |\psi_{j,m_j,n_j}(r)|^2 \int_{E^j_{m_j,n_j}}^{\infty} f(E) g^{c,s}_{j,m_j,n_j}(E) dE,$$

$$g^{c,s}_{j,m_j,n_j}(E) = \frac{1}{\pi\hbar}\sqrt{\frac{2m^{*c,s}_{z,j}}{E - E^j_{m_j,n_j}}}, \tag{4}$$

where the summation is carried out over all partially filled bands, $g_{j,m_j,n_j}(E)$ is the 1D density of states at the n_jth subband, $f(E)$ is the Fermi-Dirac distribution function, $E^j_{m_j,n_j}$ are the bottom (top) energies of the respective electron and hole subbands. Our calculations showed that for experimentally relevant pumping intensities we can only consider ground state with $m_j=0$, $n_j=0$ and two closest in energy degenerate excited states with $m_j=\pm 1$, $n_j=0$. Limiting the contribution to the charge densities only by the carriers in these states, we rewrite Eq. (4) (omitting indexes $n_j=0$) as

$$n_j(r) = \frac{|\psi_{j,0}(r)|^2}{2\pi}\int_{E^j_0}^{\infty} f(E) g^{c,s}_{j,0}(E) dE + 2\frac{|\psi_{j,1}(r)|^2}{2\pi}\int_{E^j_1}^{\infty} f(E) g^{c,s}_{j,1}(E) dE, \tag{5}$$

where E^j_0 and E^j_1 are the ground and the first excited state energies of the electron or hole, $\psi_{j,0}$ and $\psi_{j,1}$ are the wave function of the ground and first excited states, corresponding to the lowest state at $m_j=0$ and $m_j=\pm 1$; the factor 2 in the second term is due to the double degeneracy of the first excited state having the same energy for $m_j=-1$ and $m_j=1$. At zero temperature $T=0$ distribution $f(E)$ transforms into the step function and integral over E is bounded at the upper limit by the value of the quasi-Fermi energy E^j_F. For overall electrically neutral QWR the number of electrons is equal to the number of holes, $N=N_e=N_h$; thus, the linear density of the carries $n_L=N/L_z$ is related to the charge distribution as

$$n_L = \frac{2\sqrt{2}}{\pi\hbar}(\mu_{j,0}\sqrt{E^j_F - E^j_0} + 2\mu_{j,1}\sqrt{E^j_F - E^j_1}),$$

$$\mu_{j,l} = \sqrt{m^{*c}_{z,j}}\int_0^{r_c} |\psi_{j,l}(r)|^2 r dr + \sqrt{m^{*s}_{z,j}}\int_{r_c}^{r_s} |\psi_{j,l}(r)|^2 r dr, \tag{6}$$

where $\mu_{j,l}$ is a geometric average of the square root of the electron or hole effective mass arising from the mass-mismatch effect. The second term in Eq. (6) should be omitted while the respective Fermi levels E^j_F remain below the first excited state, E^j_1. In our calculations we do not introduce an additional surface charges that can arise at the interfaces between core and shell as well as between shell and vacuum due to impurities and defects. Therefore, we do not use Fermi-level pinning boundary conditions assumed, for instance, in Ref. 20. Positions of the electron and hole quasi-Fermi levels are determined in our approach by charge neutrality condition $N_e=N_h$ and Eq. (6), which relates the Fermi levels to the number of photoexcited electron-hole pairs. When solving the Poisson equation we assume zero electric field (constant potential) in vacuum outside of the structure with the zero value of the potential chosen at the core-shell interface. It should be noted that we carry out full electrostatic calculations taking into account contributions of both electrons and holes self-consistently. This circumstance distinguishes our calculations from earlier works,[22,23] where the modification of the confining potential due to the carriers was neglected within the core region, and the blueshift of the luminescence was explained only by modification of energy levels of the major carriers in the shell region due to formation of triangular quantum wells. Our calculations demonstrate that these approximations, at least for the structure considered here, are not justified, and that modification of the potential in the core region and the shift of the hole energy levels play important roles in the phenomena under study.

The self-consistent calculations are carried in the following repeated steps. At the initial step the electrostatic potential is equal to zero everywhere, i.e., $\phi(r)=0$. One-particle electron and hole wave functions calculated from Eq. (1) are used to provide the carrier concentrations as functions of radial coordinate to the Poisson equation (3). As long as the quasi-Fermi level is below the first excited state, the second term in Eq. (6) is dropped and the Fermi level is given by the following expression:

$$E^j_F = E^j_0 + \frac{\hbar^2 n_L^2 \pi^2}{8\mu^2_{j,0}}. \tag{7}$$

If, however, its value, obtained in the one-level approximation, grows above the first excited state, the second term in Eq. (6) is taken into consideration, and the value of the Fermi energy is given by a different expression,

TABLE I. Material parameters used in calculations. Here m_e^* is the mass of the electron in conduction band, m_h^* is the mass of the heavy hole in radial direction, and m_0 is the free-electron mass. Masses and dielectric constants are taken from Ref. 24 and energy values are taken from Refs. 24 and 25.

Material	m_e^*	m_h^*	ϵ	E_{gap} (eV)	ΔV_e (eV)	ΔV_h (eV)
ZnTe	$0.122m_0$	$0.60m_0$	10.3	2.39	0.35	0.78
ZnSe	$0.160m_0$	$0.75m_0$	8.60	2.82		

$$E_F^j = E_0^j + \frac{[\hbar n_L \pi \mu_{j,0} - 2\mu_{j,1}\sqrt{(\hbar n_L \pi)^2 - 8(E_1^j - E_0^j)(\mu_{j,0}^2 - 4\mu_{j,1}^2)}]^2}{8(\mu_{j,0}^2 - \mu_{j,1}^2)^2} \tag{8}$$

When a new electrostatic potential is calculated, it is substituted into the Schrödinger equation (1) and the next iteration of the self-consistent calculations continues until the convergence criteria (variation of the potential profile from iteration to iteration is smaller than a required value) is satisfied. Typically, convergence is established after 2–50 iterations, depending on the parameters of the materials in the heterojunction, the number of the excited carriers, and the uniformity of carrier distribution. If necessary, the convergence of the procedure can be improved, for instance, by taking the electrostatic potential $\phi(r)$ at a given iteration step as an average of the electrostatic potentials obtained from the previous two iterations. However, a serious problem with convergence of this scheme arises when one attempts to compute energy levels lying just below the top of the potential well. In this case, even if after a number of iterations the calculated energy levels remain inside the well reproducing type-II type of behavior, there is a chance that at the next step it will become slightly greater than the height of the well. In this situation the particle is pushed out across the interface into the second constituent material of the heterostructure resulting in large overlap of the wave functions similar to type-I heterostructures. Without the large initial separation between the carriers, the electrostatic potential reduces drastically, lowering the energy of the particle and pulling it back in its residence material. As a result, the system becomes "trapped" into a bistable state with two energy levels alternating at every iteration. This bistability, however, is an artifact of the computation method and does not correspond to any real physical effect. In our calculations this problem did not arise for moderate pumping levels. When the self-consistent solution is found the final potential profile, wave functions, electron and hole densities, and further information can be derived. The pumping intensity in our calculations was limited by the requirement that the value of the quasi-Fermi energy level (7) does not exceed the second excited state. The energy of this state is obtained from Eq. (1) by choosing the lower of two possible levels: the lowest state for angular quantum number $m_j=2$ or the second lowest state for $m_j=0$ in the potential created by the converged solution of the system. The results of our calculations for a ZnTe/ZnSe 1D structure using set of typical parameters (Table I, where m_h^* refer to effective mass of the heavy holes in the radial direction) are shown in Figs. 1 and 2.

First of these figures shows modifications of the potential profile due to photoexcited carriers for the radius of the core (ZnTe) $r_c=50$ Å and radius of the shell (ZnSe) $r_s=150$ Å. One can see that the potential profiles for both electrons and holes experience comparable modifications, which manifest in the shift of the ground-state energies for both types of carriers by about 10 meV. Plots in Fig. 2 give more detailed description of the dependence of energy characteristics of electrons and holes on the number of excited pairs. First of all we shall note that the deviation of the quasi-Fermi level of holes from E_0^h is very small even when the vertical effective mass of the holes is chosen equal to the in-plane mass. The electron quasi-Fermi level, on the contrary, depends

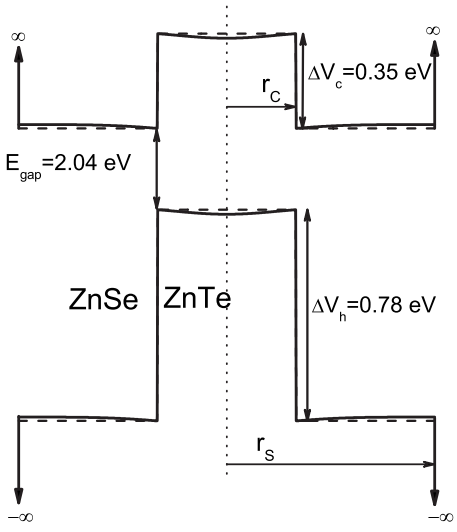

FIG. 1. Band energy diagram of the ZnTe/ZnSe type-II core-shell quantum wire with core radius 50 Å and shell radius 150 Å. Dashed lines represent the diagram in the absence of the free carriers, for which the electron ground energy $E_0^e=19$ meV and the hole ground energy $E_0^h=13$ meV. Solid lines are the potential profiles for linear density $n_L=7\times10^7$ m^{-1} with $E_0^e=31$ meV and $E_0^h=24$ meV. Energy values are counted from the bottom of each unaffected well. All profiles are in scale except of the gap between conduction and valence bands.

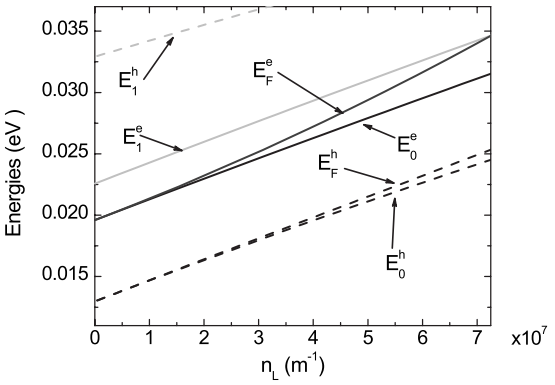

FIG. 2. Dependence of the energies of the ZnTe/ZnSe type-II core-shell quantum wire (r_c=50 Å and r_s=150 Å) on the density of the carries. The gap energy is not added. The maximum value of the density is limited by the condition for the quasi-Fermi level to be below the first excited state. The solid curves represent the electron energy levels: ground state, quasi-Fermi state (black), and first excited state (gray). The dashed curves show the same for holes. Hole quasi-Fermi energy level is shown for the same mass of the hole along the z direction as the mass along radial direction.

quite significantly on the number of electrons, and one can see in Fig. 1 that at some level it exceeds the energy of the excited level of the electrons. The main qualitative conclusion of these calculations is that the nonuniform distribution of the holes in these samples and its modification with the concentration of the carriers significantly affects the potential profile and energy levels of the electron-hole pairs and, therefore, has to be taken into account.

In order to calculate the complete spectral profile of the luminescence intensity one would need to integrate over all states involved in transition taking into account their joint density of states. In this work, however, we have a more modest goal to analyze overall spectral shift of the PL with pumping intensity. To this end, it is sufficient to consider the pumping dependence of the maximum and minimum energies of the emitted photons defined as

$$\hbar\omega_{\max} = E_{e,F} - E_{h,F} + E_{\text{gap}},$$

$$\hbar\omega_{\min} = E_{e,0} - E_{h,0} + E_{\text{gap}}, \tag{9}$$

where E_{gap} is defined in Fig. 1.

B. Time dependence of luminescence intensity

We analyze the time dependence of luminescence assuming that only electron and hole subbands originating from their respective ground states with m_j=0 are populated and that the radiative recombination occurs between electron and holes occupying the respective ground-state subbands. Neglecting changes in the number of electron-hole pairs due to nonradiative recombination (case of low temperature), kinetics of the number of carriers is described by a simple equation,

$$\frac{dn_L(r_c,r_s,t)}{dt} = -\frac{n_L(r_c,r_s,t)}{\tau(r_c,r_s,n_L)}, \tag{10}$$

where τ^{-1} is the rate of the radiative spontaneous recombination of the electron-hole pairs. In this equation we explicitly indicate the dependence of the carrier density and τ on the radii of the core-shell structure anticipating subsequent averaging over their distributions. The recombination rate is given by the Fermi golden rule and is proportional to the overlap integral,

$$\tau(r_c,r_s,n_L)^{-1} = R|\langle\psi_{e,0}|\psi_{h,0}\rangle|^2. \tag{11}$$

The constant R includes all microscopic constants such as the dipole matrix element calculated between the Bloch functions of the conduction and valence bands, which do not depend on the pumping intensity or geometry of the structure. The overlap integral between the envelope wave functions $\psi_{e,0}$ and $\psi_{h,0}$ is the only parameter which does depend on the radii of the core-shell structure and on the number of the existing electron-hole pairs.

In the case of the ensemble of nanostructures the observable PL intensity is determined by the average over the ensemble number of the electron-hole pairs, which can be expressed in terms of distribution functions f_c and f_s of the core and shell radii[14] as follows:

$$\bar{n}_L(t) = \int_{\bar{r}_c-\Delta_c}^{\bar{r}_c+\Delta_c}\int_{\bar{w}-\Delta_w}^{\bar{w}+\Delta_w} n_L(r_c,r_c+w,t)f_c(r_c)f_w(w)dr_c dw, \tag{12}$$

where $w=r_s-r_c$ is the width of the shell, $\bar{r}_c$ and $\bar{w}$ are average values of the respective quantities, and Δ_c and Δ_w determine their maximum and minimum values used for numerical evaluation of the respective integrals. The normalized PL intensity I_{PL} at a given photon energy, is defined by the rate of change in the average number of electron-hole pairs,[14]

$$I_{\text{PL}}(t) = -\frac{1}{\bar{n}_L(0)}\frac{d\bar{n}_L(t)}{dt}, \tag{13}$$

where $\bar{n}_L(0)$ is an average concentration of the carriers at initial moment of time t=0. If one takes into account the dependence of the decay time τ on the concentration n_L, the solution of Eq. (10) is no longer given by an exponential function and can only be found numerically. In order to characterize this solution it is convenient to use a quantity

$$\tau_0 = \lim_{n_L\to 0} \tau(n_L,\bar{r}_c,\bar{r}_s).$$

This parameter characterizes the decay rate at vanishingly small concentration of the carriers (the flat-band condition) in a structure with average geometric parameters. With the use of this quantity one can present the dimensionless quantity $\eta(n_L,r_s,r_c)$ defined as

$$\eta(n_L,r_c,r_s) = \frac{\tau}{\tau_0}.$$

This quantity does not depend on microscopic characteristics of the materials constituting the structure [represented by factor R in Eq. (11)] and only retains dependence on the

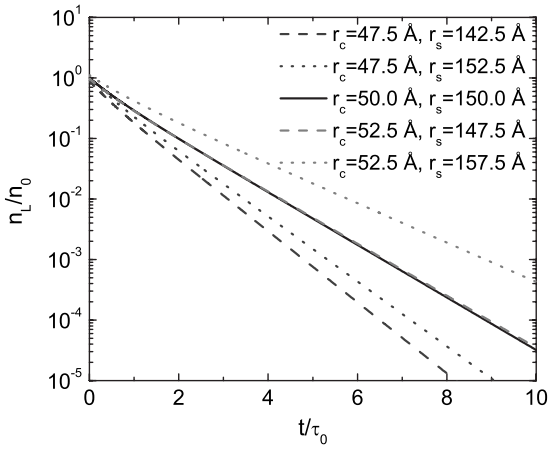

FIG. 3. Time dependence of the normalized population of the ground subbands of the ZnTe/ZnSe type-II core-shell quantum wires for different geometrical parameters of the structure. The solid black curve corresponds to the structure with core radius of 50 Å and shell radius of 150 Å. The light and dark gray dashed and dotted curves correspond to the variation of the core and shell radii. The time scale is normalized by τ_0, calculated lifetime from the tail of the population dynamics of the structure (r_c=50 Å and r_c=150 Å).

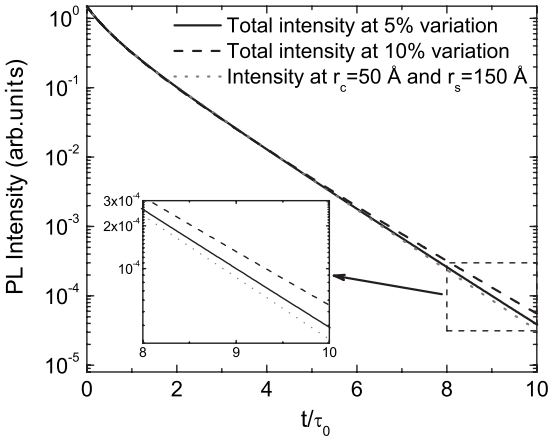

FIG. 4. Time decay of the PL intensity of the ensemble of ZnTe/ZnSe type-II core-shell quantum wires with distribution of the inner radius around core radius of 50 Å and distribution of the thickness of the shell region around 100 Å. The gray dotted line shows the PL decay for the core-shell quantum wire with r_c=50 Å and r_s=150 Å. The solid curve shows intensity of the 5% variation of the radii. The dashed curve represents 10% variation of the geometrical parameters.

excitation intensity and the radii of the core and the shell. To illustrate the effect of the difference in the core-shell radii on population dynamics, we solved Eq. (10) for several different values of r_c and r_s. The results of the calculations are shown in Fig. 3, where time t is normalized by parameter τ_0 calculated at the radii values r_c=50 Å and r_s=150 Å. The chosen values of the parameters correspond to typical colloidal quantum wire systems.[26] The curves shown in Fig. 3 are characterized by different initial densities, which is due the fact that for wires with different cross sections the linear density will differ even if the respective volume densities are the same. For all initial densities in these calculations the quasi-Fermi levels are below the first excited states for both electrons and holes. These calculations demonstrate that even small changes in the geometry of the system affects the decay rate of the population, so that in realistic samples the distribution of radiative rates due to size dispersion of the structures significantly affects the PL decay. In order to find the time dependence of PL in this case we need to evaluate the following expression:

$$I_{\mathrm{PL}}(t) = -\frac{1}{\bar{n}_L(0)\tau_0}\int_{\bar{r}_c-\Delta_c}^{\bar{r}_c+\Delta_c}\int_{\bar{w}-\Delta_w}^{\bar{w}+\Delta_w}\frac{n_L(t,r_c,r_c+w)}{\eta(t,r_c,r_c+w)} \times f_c(r_c)f_w(w)dr_c dw \tag{14}$$

which requires solving Eq. (13) for large number of different values of r_s and w randomly chosen from a specified distribution. We will assume that r_c and w are independent random Gaussian variables with variances determined by the growth technology. This description of the radii is consistent with manufacturing process of the colloidal wires.[26] Standard deviations $\sigma_{(c,w)}$ for both distributions are defined in terms of Δ_c and Δ_w as $\Delta_{c,w}=3\sigma_{c,w}$, while $\Delta_{c,w}$ are determined via relative maximum deviation $\Delta_r=\Delta_c/\bar{r}_c=\Delta_w/\bar{r}_w$. Results of the calculations carried out for Δ_r=5% and Δ_r=10% are presented in Fig. 4. The gray dotted line shows the PL decay of the core-shell structure without any variations of the radii. At large time scales the tail of the decay is a single exponent as it supposed to be for almost constant lifetime. The solid black curve shows the decay of intensity at Δ_r=5%, while the dashed curve corresponds to Δ_r=10%. At earlier times all curves exhibit significantly fast decay, which at longer times slows down. Such a behavior is qualitatively explained by the large overlap of electron and hole wave functions immediately after excitation due to strong band bending caused by increased carrier density. This density decreases with time due to recombination resulting in the decrease in the electron-hole overlap and slower rate of recombination. It is interesting that in the strong band bending regime the time dependence of the luminescence appears only weakly dependent on the size disorder. At later times, however, when in the absence of disorder one would have observed a standard exponential decay, the deviations from the exponential behavior persist, but are now strongly dependent on the size dispersion. For larger disorder the time dependence of PL is much slower resulting in a longer tail of the PL. Thus our calculations reveal that the two sources of the nonexponential behavior manifest themselves at different time scales: effects due to carrier concentration prevail at shorter times, while the disorder determines the kinetics of luminescence at longer times.

III. COMPARISON WITH EXPERIMENTAL RESULTS FOR VERTICALLY STACKED QUANTUM DOTS

Here we compare the theory presented in Sec. II with experimental results obtained for vertical stacks of quantum dots. The experiments were conducted with multiple stacked ZnTe/ZnSe type-II QDs (Fig. 5) grown by migration-

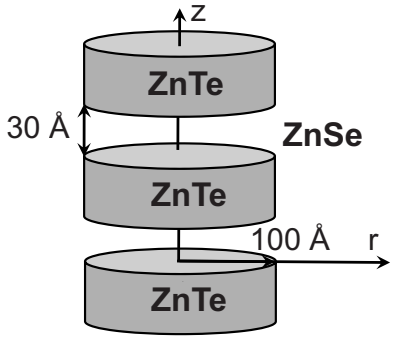

FIG. 5. Schematic representation of the stacked quantum dots with their typical spatial parameters.

enhanced epitaxy, with growth period of 3 nm as confirmed by x-ray diffraction.[27] Details of the growth procedure can be found elsewhere.[15,27,28] The cw PL was performed in the usual configuration using the 325 nm line of a He-Cd laser, a $\frac{3}{4}$ m monochromator, and a thermoelectrically cooled GaAs photomultiplier coupled with a SR400 photon counter. The excitation intensity was varied over 4 orders of magnitude using neutral density filters. In the time-resolved PL measurements, a N_2 laser (4 ns pulse width) and a 500 MHz bandwidth TDS 654C oscilloscope were used for excitation and detection, respectively. All measurements were done in a closed-cycle refrigerator system at 10 K. Results of cw PL measurements of the sample studied previously by time-resolved PL in Ref. 10, and for which exciton binding energy is 2 meV, are shown in Fig. 6 for several excitation intensities. Figure 7 demonstrates the shift of the PL emission energies [Eq. (9)] as a function of the pumping intensity. Solid squares and triangles show shift of emission frequencies corresponding to the intensity of luminescence equal to 20% of the maximum intensity on the lower- and higher-energy sides of the PL band, respectively. We chose to focus on these energies instead of commonly used peak energies in order to eliminate contribution to the luminescence from excitons bound to isoelectronic centers (ICs) of different sizes, which are known to contribute significantly to the higher-frequency side of the PL band emitted by type-II QDs.[9] Recently, it has

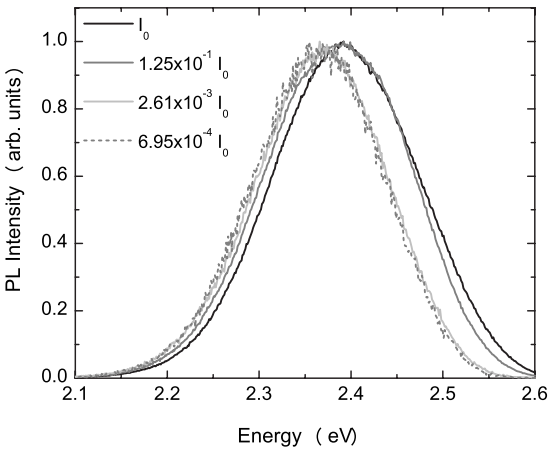

FIG. 6. PL spectra obtained for sample at four different intensities of excitation.

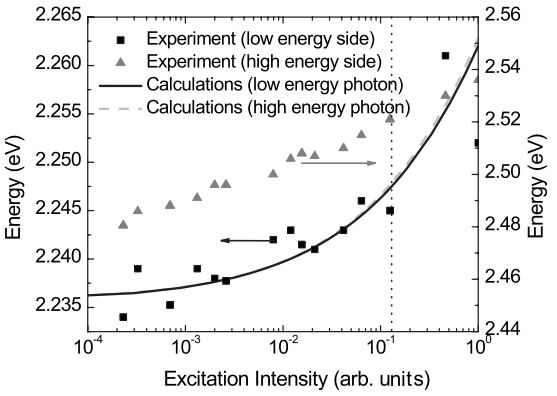

FIG. 7. Dependence of the emission energy on the normalized excitation intensity. The light gray dashed line represents the maximum energy (left vertical axis) of the electron-hole transition between quasi-Fermi energy levels [Eq. (9)], while the solid black line corresponds to the minimum energy of the band-to-band transition (same axis). The black squares correspond to the experimental emission energy (left vertical axis) taken at 20% height of the peak on the low-energy side. The gray triangles show the energy (right vertical axis) taken at the same height, but from the high-energy side of the PL spectra. The vertical dotted line shows excitation intensity ($I^{\mathrm{exc}} \sim n_L^2$) for which electron quasi-Fermi energy level reaches the first excited state.

also been pointed out that this spectral region can also be affected by possible Mott transition which might take place at high excitation intensities.[29] Focusing on frequencies from lower-energy part of the PL line, we are able to minimize the undesirable contribution from these effects, which masks the properties under study in this work. Behavior of a frequency chosen from the higher-energy side of the band is shown for comparison and can be seen to be qualitatively different. This frequency shifts with increased pumping significantly faster because at higher pumping power the contribution from isoelectronic bound excitons is greater, resulting in an apparent shift toward higher frequencies. Similar effect has been also observed in magneto-PL,[15] where effects associated with type-II QDs were obvious only at relatively low excitation intensities.

Therefore we compare our theoretical results obtained from Eqs. (7)–(9) with the behavior of the lower-energy side of the PL. For calculations we used the same material parameters as previously (Table I) with only difference that now we use an independent hole effective mass in the vertical direction. The value of this mass is not known, and we use it together with band offsets as a fitting parameter. Also, we take into account that in the experimental samples the radius of the core is $r_c = 100$ Å (Refs. 15 and 16) and the shell is virtually infinite. In order to imitate this situation theoretically we chose $r_s = 1000$ Å. Calculated results are shown by the solid line, which, as expected, reproduces proportionality of the shift to the cubic root of the pumping intensity and can be fitted to provide a good agreement with the experimental results.

While the shift of the PL with pumping intensity for type-II nanostructures has been extensively discussed in the literature,[6–8,10] the time evolution of the PL has so far at-

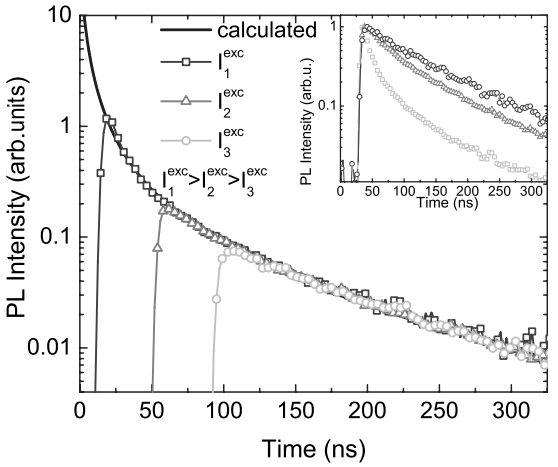

FIG. 8. Time dependence of the PL intensity for different excitation intensities. The solid line corresponds to the intensity obtained from Eq. (13) with 5% variation of the core radius r_c around 100 Å. Symbols show measured time-resolved PL for three different excitation intensities. The time scale is for data obtained at the highest excitation intensity. The inset shows these decays as normalized curves (the time scale is in reference to the laser pulse for each intensity).

tracted much less attention. Although there are works where PL lifetime has been calculated as a function of the photoexcited carrier concentration and PL kinetics in quantum wells was compared with experiment (see, e.g., Refs. 6 and 30), we are not aware of any work related to the structures with cylindrical symmetry and dispersion of the geometrical parameters. Inset of Fig. 8 shows normalized time-resolved PL at 2.385 eV (low-energy side of the PL) for three different excitation intensities. At the lowest excitation intensity the PL curve exhibits a decay that is close to a single exponential, but does not appear to be as exact one. The PL decay obtained at higher excitation intensities is significantly nonexponential in agreement with previous experiments[6,9,10] and our theoretical results presented in Fig. 4.

The three curves shown in inset of this figure can be rescaled and plotted as a single curve. Indeed, the higher pumping power creates the larger concentration of the carriers at $t=0$. However, at some later instance t_1 this concentration, which continuously decreases, will become equal to the initial concentration of the carriers at the lower pumping. Therefore, by simply shifting the point $t=0$ to $t=t_1$ the respective lower pumping curve must coincide with the part of the higher pumping curve for $t>t_1$. Shifting initial times for all three curves in the inset, we obtain the master curve shown in main Fig. 8. One can see that points from all three different pumping intensities form a perfect single line, which shows excellent agreement with the results of the theoretical calculations depicted by the solid line. This line presents a normalized PL intensity obtained from Eq. (14) with $\Delta_r=5\%$, $\bar{r}_c=100$ Å, and $\tau_0=140$ ns. Such a small size distribution is consistent with our main assumption that vertically stacked QDs can be treated as a one-dimensional system. Indeed, 5% size distribution is much smaller than the actual distribution of the constituent QDs, which can only be explained by averaging out of the dot diameters due to expanded nature of the wave functions of the carriers. A large value for τ_0 is consistent with type-II band alignment in ZnTe/ZnSe heterostructures.

Finally, we would like to note that the theoretical curve in Fig. 8 demonstrates much faster decay of the luminescence than the curve in Fig. 4 at earlier times, but with slower decrease in intensity at the longer times. This distinction is due to difference in the shell radii used to obtain these two figures. In the case of Fig. 4 we dealt with very wide shell layer, so that the overlap of the electron-hole wave functions, even though small to begin with, is much more sensitive to the changes in the band structure. It, therefore, decreases much faster with the concentration, and hence with time, than in the case of Fig. 4, which describes decay of PL in the sample with a much narrower shell. At the same time, the fast decrease in the overlap makes instantaneous values of the decay rate much smaller resulting in a much slower decay at longer times.

IV. SUMMARY

In this paper, we have calculated the electron and hole states and confining potential for cylindrical type-II core-shell structures from a numerical solution of the self-consistent Schrödinger-Poisson system of equations. We measured cw and time-resolved PL from ZnTe/ZnSe vertically stacked type-II QDs. We analyzed PL kinetics in such a system taking into account the size dispersion of the nanostructures. The results of calculations are found to be in a good agreement with the experimental observations. The observed time-resolved PL is described quantitatively, which allowed one to obtained numerical value for the parameter τ_0, characterizing overlap of the electron and hole wave functions in the flat-band limit. The discrepancy in cw PL spectra at high excitation levels is explained by the emission of the isoelectronic bound excitons, which are always present in Zn-Se-Te systems. We also discussed and investigated a model situation for the core-shell structure with finite thickness of the shell applicable to the colloidal quantum wires. It was shown that with the existence of the distribution of the radii the PL decay has essentially nonexponential behavior even at the tail of the decay where the carrier lifetime is almost the same due to slowly changing overlap of the electron and hole wave functions. We expect that our results will spur experimental time-resolved studies in such colloidal systems.

ACKNOWLEDGMENTS

We would like to acknowledge support from DOE under Grant No. DE-FG02-05ER46219 and from AFSOR under Grant No. FA9550-07-1-0391.

[1] Y. Huang, X. Duan, Y. Cui, and C. M. Lieber, Nano Lett. **2**, 101 (2002).
[2] H.-J. Choi, J. C. Johnson, R. He, S.-K. Lee, F. Kim, P. Pauzauskie, J. Goldberger, R. J. Saykally, and P. Yang, J. Phys. Chem. B **107**, 8721 (2003).
[3] F. Qian, S. Gradečak, Y. Li, C.-Y. Wen, and C. M. Lieber, Nano Lett. **5**, 2287 (2005).
[4] L. J. Lauhon, M. S. Gudiksen, D. Wang, and C. M. Lieber, Nature (London) **420**, 57 (2002).
[5] Y. Wu, R. Fan, and P. Yang, Nano Lett. **2**, 83 (2002).
[6] S. V. Zaitsev, A. A. Maksimov, I. I. Tartakovskii, D. R. Yakovlev, M. Bayer, and A. Waag, Phys. Rev. B **76**, 035312 (2007).
[7] C. Y. Jin, H. Y. Liu, S. Y. Zhang, Q. Jiang, S. L. Liew, M. Hopkinson, T. J. Badcock, E. Nabavi, and D. J. Mowbray, Appl. Phys. Lett. **91**, 021102 (2007).
[8] D. Alonso-Álvarez, B. Alén, J. M. García, and J. M. Ripalda, Appl. Phys. Lett. **91**, 263103 (2007).
[9] Y. Gu, I. L. Kuskovsky, M. van der Voort, G. F. Neumark, X. Zhou, and M. C. Tamargo, Phys. Rev. B **71**, 045340 (2005).
[10] Y. Gu, I. L. Kuskovsky, M. van der Voort, G. F. Neumark, X. Zhou, M. Munoz, and M. C. Tamargo, Phys. Status Solidi B **241**, 515 (2004).
[11] K. Hantke, J. D. Heber, C. Schlichenmaier, A. Thränhardt, T. Meier, B. Kunert, K. Volz, W. Stolz, S. W. Koch, and W. W. Rühle, Phys. Rev. B **71**, 165320 (2005).
[12] J. Enderlein and R. Erdmann, Opt. Commun. **134**, 371 (1997).
[13] M. N. Berberan-Santos, E. N. Bodunov, and B. Valeur, Chem. Phys. **315**, 171 (2005).
[14] A. F. van Driel, I. S. Nikolaev, P. Vergeer, P. Lodahl, D. Vanmaekelbergh, and W. L. Vos, Phys. Rev. B **75**, 035329 (2007).
[15] I. L. Kuskovsky, W. MacDonald, A. O. Govorov, L. Muroukh, X. Wei, M. C. Tamargo, M. Tadic, and F. M. Peeters, Phys. Rev. B **76**, 035342 (2007).
[16] I. R. Sellers, V. R. Whiteside, I. L. Kuskovsky, A. O. Govorov, and B. D. McCombe, Phys. Rev. Lett. **100**, 136405 (2008).
[17] P. C. Sercel and K. J. Vahala, Appl. Phys. Lett. **57**, 545 (1990).
[18] F. V. Kyrychenko and J. Kossut, Phys. Rev. B **61**, 4449 (2000).
[19] L. Wang, D. Wang, and P. M. Asbeck, Solid-State Electron. **50**, 1732 (2006).
[20] J. H. Luscombe, A. M. Bouchard, and M. Luban, Phys. Rev. B **46**, 10262 (1992).
[21] C. R. Proetto, Phys. Rev. B **45**, 11911 (1992).
[22] A. Shik, H. Ruda, and E. H. Sargent, Nanotechnology **12**, 523 (2001).
[23] N. N. Ledentsov *et al.*, Phys. Rev. B **52**, 14058 (1995).
[24] O. Madelung, *Semiconductors: Data Handbook*, 3rd ed. (Springer, New York, 2004).
[25] D. Segev and S.-H. Wei, Phys. Rev. B **68**, 165336 (2003).
[26] A. Dong, H. Yu, F. Wang, and W. E. Buhro, J. Am. Chem. Soc. **130**, 5954 (2008).
[27] Y. Gong, W. MacDonald, G. F. Neumark, M. C. Tamargo, and I. L. Kuskovsky, Phys. Rev. B **77**, 155314 (2008).
[28] Y. Gu, I. L. Kuskovsky, and G. F. Neumark, *ZnSeTe Rediscovered: From Isoelectronic Centers to Quantum Dots in Wide Bandgap Light Emitting Materials and Devices* (Wiley, New York, 2007).
[29] B. Bansal, M. Hayne, M. Geller, D. Bimberg, and V. V. Moshchalkov, Phys. Rev. B **77**, 241304(R) (2008).
[30] A. A. Maksimov, S. V. Zaitsev, I. I. Tartakovskii, V. D. Kulakovskii, N. A. Gippius, D. R. Yakovlev, W. Ossau, G. Reuscher, A. Waag, and G. Landwehr, Phys. Status Solidi B **221**, 523 (2000).